Received 21 March 2024; revised 24 April 2024; accepted 1 May 2024. Date of publication 6 May 2024; date of current version 20 May 2024.

Digital Object Identifier 10.1109/OJUFFC.2024.3397630

Development of an Air-Coupled Piezoelectric Micromachined Ultrasonic Transducer Using Sol-Gel PZT Thin Film for Fast-Prototyping

YA-HAN LIU[1], (Graduate Student Member, IEEE), HSIAO-CHI LIN[2], CHIH-YING LI[2], CHIEN-LUN KAO[2], HAN-JEN HSU[2], YEONG-HER WANG[1], (Life Member, IEEE), AND CHIH-HSIEN HUANG[2], (Member, IEEE)

[1]Institute of Microelectronics, National Cheng Kung University, Tainan 701401, Taiwan
[2]Department of Electrical Engineering, National Cheng Kung University, Tainan 701401, Taiwan

CORRESPONDING AUTHORS: C.-H. HUANG (chihhsien_h@mail.ncku.edu.tw) and Y.-H WANG (yhw@ee.ncku.edu.tw)

This work was supported in part by the National Science and Technology Council (NSTC) under Grant NSTC 112-2218-E-006-010-MBK; and in part by the Core Facility Center, National Cheng Kung University, Taiwan.

ABSTRACT This study demonstrated the first air-coupled pMUT using sol-gel PZT thin film that could deliver ultrasonic waves to mid-air. First, the deposition conditions for making PZT thin film with high remanent polarization were determined. Then, air-coupled pMUTs with resonance frequencies close to 40 kHz were designed using the circular plate model. According to the design, pMUTs with radii measuring 600 μm to 775 μm were fabricated to evaluate the acoustic output pressure. Among these, the pMUT with the 725 μm radius achieved a maximum sound pressure output of 4.42 Pa at 3 cm above when driven with 10 Vpp, and the resonance frequency was 40.48 kHz. Finally, the output pressure of a phased array consisting of sol-gel PZT-based pMUTs with a 725 μm radius was calculated using the k-Wave toolbox. The output pressure of the 11 $\times$ 11 pMUT array reached 365.62 Pa when focused at 3 cm above it. This result revealed that the output pressure of the proposed pMUT array could fulfill the requirement for most mid-air ultrasound applications.

INDEX TERMS Sol-gel deposition, airborne piezoelectric micromachined ultrasonic transducers.

I. INTRODUCTION

OVER the past 70 years, ultrasonic transducers have been widely applied in industrial and biomedical applications, such as nondestructive evaluation [1], [2], medical imaging [3], [4], and non-invasive treatments [5], [6]. Along with the development of semiconductor fabrication and integrated circuits, analog and digital circuits for multichannel phase delay systems have become popular. Several state-of-the-art mid-air ultrasonic applications were achieved using hundreds of transducers, including ultrasonic haptic feedback [7], [8], acoustic particle manipulation [9], and gesture recognition [10]. Acoustic signals decay rapidly in the air, and the attenuation coefficient is proportional to the working frequency. Hence, most mid-air ultrasonic applications use frequencies between 20 kHz and 100 kHz. However, commercial air-coupled ultrasonic transducers are usually bulky and hard to be integrated into consumer electronics, thus hindering further development of these mid-air ultrasonic applications.

In recent decades, the development of micro-electro-mechanical system technology has provided researchers with an alternative method to fabricate ultrasound transducers [11]. Compared with traditional transducers, MUTs are more capable of integrating air-coupled ultrasonic systems into commercial electronic devices. Currently, two types of MUTs, capacitive micromachined ultrasonic transducers (cMUTs) and piezoelectric micromachined ultrasonic transducers (pMUTs) are being explored as replacements for conventional piezoelectric ultrasonic transducers. The cMUT is driven with electrostatic force and formed by suspending a membrane coated with the top electrode above a substrate with a bottom electrode. Hence, it requires a precise and uniform micrometer scale gap between the top and bottom electrodes to have satisfactory sensitivity [12]. However, the

size of the diaphragm would need to increase to achieve lower frequency for mid-air applications. Such an extreme gap is very challenging to fabricate when the dimension of the membrane increases. Besides, the cMUT requires a high DC bias voltage to drag the membrane to increase the transmitting/receiving efficiency, which might cause some safety issues in consumer electronics. In contrast, pMUTs do not require a bias voltage or a delicate gap. Hence, they are considered a better candidate for implementing mid-air ultrasonic applications in consumer electronic devices. A pMUT consists of a suspended membrane sandwiched between a top electrode/piezoelectric material layer and a bottom electrode/structural layer. When an AC voltage is applied to the piezoelectric layer through the electrodes, the membrane vibrates the medium and generates sound waves due to the lateral strain induced by the piezoelectric effect. To date, pMUTs with different piezoelectric materials and fabrication methods have been used in various ultrasonic applications in the air, such as mid-air haptics applications, long-range detection, and acoustic hologram [8], [10], [13].

As an excitation layer, the piezoelectric material plays a crucial role in pMUT technology. Polyvinylidene fluoride (PVDF), aluminum nitride (AlN), and lead zirconate titanate (PZT) are the three primary materials for pMUT. Halbach et al. proposed a potentially transparent pMUT with PVDF as the piezoelectric layer to achieve mid-air ultrasonic haptic feedback [8]. However, the output acoustic pressure was not enough to be felt by the human finger because the piezoelectric coefficient of PVDF was not large enough. Luo et al. presented a pMUT array for long-range detection in the air using PZT deposited with physical vapor deposition as the actuation layer [13]. The acoustic pressure per unit volume was almost 25 times larger than the commercial bulk-PZT transducer (Murata Manufacturing, MA40S4S). Their results highlighted the possibility of replacing the conventional air-coupled ultrasonic transducer with PZT-based pMUT for miniature ultrasonic systems.

Currently, the sol-gel method, radio-frequency magnetron sputtering (RF sputtering), and pulsed laser deposition (PLD) are the most common methods for fabricating PZT thin films. Both RF sputtering [14] and PLD [15] require expensive equipment and operate under vacuum; in contrast, the sol-gel process has less stringent requirements for the facility [16], [17]. Therefore, the sol-gel method is more friendly for the initial development and experimental verification stages of designing pMUTs for novel mid-air ultrasonic applications. Although some air-coupled pMUTs made by sol-gel PZT thin film have been demonstrated, they were not designed for mid-air applications, which required the transducers to transmit or receive ultrasonic waves to or from the air medium [18.19]. Besides, the resonance frequency of commercial ultrasonic transducers for mid-air applications such as haptic feedback, object detection, and particle manipulation was usually between 20 and 100 kHz, which hasn't been discussed in previous works. Hence, this study proposed an air-coupled pMUT dedicated to mid-air ultrasonic applications with resonance frequency of 40kHz using a PZT layer fabricated with the sol-gel process. To improve the piezoelectric coefficients of PZT thin films, the deposition and annealing processes for sol-gel PZT thin films were optimized first. Next, a fabrication process was investigated to build high throughput pMUTs with resonance frequencies around 40 kHz. Finally, the characterizations of the PZT thin film and pMUT were performed, followed by a simulation that evaluated the focused acoustic pressure generated by the pMUT array.

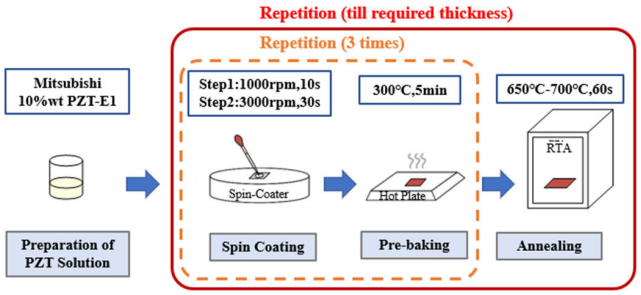

FIGURE 1. **Fabrication process of the sol-gel-based PZT thin film.**

The following section describes the deposition process of the sol-gel PZT thin film, as well as the design, modeling, and fabrication of air-coupled pMUTs. Section III discusses the characterization results of the fabricated PZT thin films and pMUTs and the simulation results to evaluate the output pressure of a phased pMUT array. The final section concludes this research and discusses the potential of using pMUTs actuated by sol-gel PZT thin film for mid-air ultrasonic applications.

II. METHOD

A. FABRICATION AND CHARACTERIZATION of the SOL-GEL PZT THIN FILM

To demonstrate the sol-gel PZT-based pMUT, this study used a commercial precursor to deposit a PZT thin film as the actuation layer for the pMUT. According to previous research, the thermal expansion coefficient of Pt is similar to that of PZT, which prevents cracks during rapid thermal annealing [20]. Hence, 20 nm Ti and 250 nm Pt were deposited onto a Si substrate by e-beam evaporation in this study, where Ti served as the adhesion layer. Figure 1 presents the process of depositing the PZT film using the sol-gel method. After preparing the substrate, 1.5 ml metal alkoxide precursor (10% PZT [110/52/48] E1, Mitsubishi Material, Japan) was put on a 6-inch wafer. Then, the sol-gel solution was first spun at 1000 rpm for 10 s to uniformly distributed on the substrate, followed by 3000 rpm for 30 s to reach the required thickness. The sample was then dried and pyrolyzed at 300 °C for 5 min to remove the organics in the precursor solution to convert the deposited PZT film from amorphous to crystallized.

This process was repeated two more times for rapid thermal annealing. Finally, 60 s of rapid thermal annealing (RTA) was applied to polarize the sol-gel thin film by converting the

crystallization from pyrochlore to perovskite. The maximum temperature of RTA was set at various points between 650 °C and 700 °C to observe the results of remnant polarization and surface cracks. The entire coating step was repeated several times to reach the required thickness. As an electrical actuation and receiving device, the piezoelectric layer of the pMUT had to be sandwiched between the top and bottom electrodes. The Pt deposited on the substrate before coating the PZT thin film could also serve as the bottom electrode. To expose the bottom electrode, part of the PZT thin film was removed using a two-step wet-etch patterning process [21]. Firstly, the wafer was patterned using photolithography and immersed in a buffered oxide etchant (the ratio of 40% NH_4F in water to 49% HF in water was 6:1) to react with the PZT in the exposed region. Then, HCl was used to remove the reactants of the previous step. Finally, the 100 nm Al top electrode was patterned using RF sputtering and lift-off.

To evaluate the film thickness after each spin coating, a sample with 27 PZT layers was prepared, and a wet etching was performed to expose the underlying Pt electrode. Afterward, a profilometer (Alpha-Step) was used to measure the thickness. Besides, to observe the crystallization of the PZT films under different annealing parameters, the crystalline structures were examined using an X-ray diffractometer (XRD, Bruker D8 Discover). The performance of a piezoelectric material is usually determined by the remnant polarization value (P_r) to indicate the amount of polarization (charges per area) that remained in the material without an electric field. Therefore, a ferroelectric tester (Precision LC II) was used to record the polarization-electric field hysteresis loops (P-E loop) and identify the value of remnant polarization.

The transverse piezoelectric coefficient (d_{31}) of a pMUT's actuation layer is directly related to its driving and receiving efficiency. By standard notation, the indices 1, 2, and 3 correspond to the x, y, and z coordinate axes, respectively (Figure 2). Therefore, d_{31} represented the lateral contraction level of the film when a voltage is applied between the top and bottom electrodes. As shown in Figure 2, the 700 μm wafer coated with sol-gel PZT thin film and electrodes was diced to make a 20 mm × 3 mm cantilever to evaluate the d_{31} of the proposed piezoelectric thin film. According to a previous study, the transverse piezoelectric coefficient d_{31} can be calculated by

$$d_{31} \cong -\frac{h_s^2 Y_s (s_{11}^E + s_{12}^E)}{3(1-v_s)L^2 V}\delta \tag{1}$$

where (δ) is the tip displacement measured via laser Doppler vibrometer (LDV); h_s is the thickness of the substrate; Y_s and Y_p are Young's modulus of the substrate and the piezoelectric layer, respectively; v_s and v_p are Poisson's ratio of the substrate and piezoelectric layer; L is the length of the top electrode; and V is the applied voltage [22]. The elastic compliance coefficients s_{11}^E and s_{12}^E represent the induced strain of the material corresponding to the electrical field, and

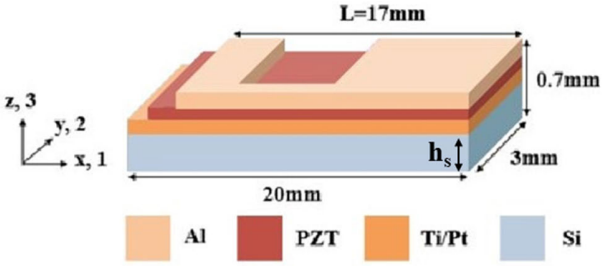

FIGURE 2. Schematic drawing of the cantilever.

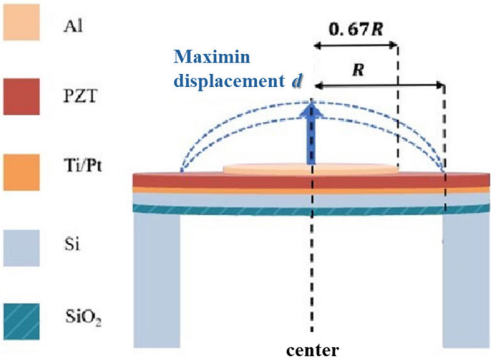

FIGURE 3. Structure of the proposed pMUT.

they are obtained by

$$s_{11}^E = \frac{1}{Y_p}, s_{12}^E = -\frac{v_p}{Y_p} \tag{2}$$

B. DESIGN OF A SINGLE pMUT

After the deposition process of the sol-gel PZT thin film was optimized, this study demonstrated the feasibility of using this thin film to make a 40 kHz pMUT. As Figure 3 shows, the proposed pMUT had a circular shape, and its dimension was defined by the radius of the back cavity (R). To achieve the best driving efficiency in the first vibration mode, the radius of the actuation region (where the top and bottom electrodes overlap) was set to 67% of the cavity's radius, based on previous research [14], [23]. The stack of the pMUT consisted of the piezoelectric layer, electrode layers, and elastic support layer. The deformation of the membrane along the longitudinal axis generates an acoustic pressure due to the transverse stress of the piezoelectric layer when an electric field is applied. Aside from the actuation region, the thickness of the piezoelectric layer also affects the efficiency of the pMUT for a given radius. Hence, this study used the circular plate model to find the radius of a 40 kHz pMUT and optimize the thickness of its piezoelectric layer [24]. According to the model, the pMUT stack has n layers, as shown in Figure 4. z_n indicates the height from the bottom plane to the top of the n_{th} layer. h_n and ρ_n are the thickness and mass density of the n_{th} layer, respectively. Consequently, the resonance frequency of

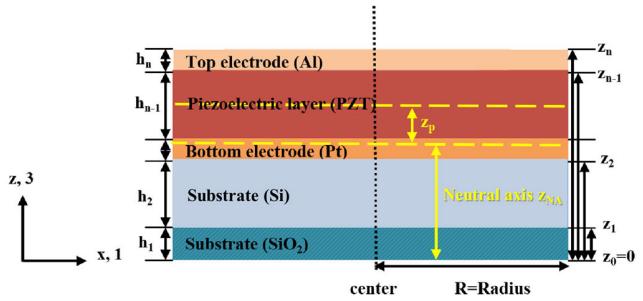

FIGURE 4. **Circular plate model of the proposed pMUT.**

the pMUT can be calculated by:

$$f = \frac{\lambda^2}{2\pi R^2}\sqrt{\frac{D}{I_0}} \tag{3}$$

$$I_0 = \sum_{n}^{N} \rho_n h_n \tag{4}$$

$$D = \sum_{n}^{N} \frac{E_n}{3(1-\nu_n^2)}\left[(z_n - z_{NA})^3 - (z_{n-1} - z_{NA})^3\right], \tag{5}$$

where R is the radius of the pMUT; λ is the axisymmetric vibration mode constant; I_0 is the mass per unit area; and D is the flexural rigidity. Young's modulus of the material, Poisson's ratio of each layer, and the height of the neutral axis are denoted as E_n, ν_n, and z_{NA}, respectively.

The maximum displacement d at the center of a clamped circular plate can be estimated by:

$$d = \frac{3R^2\eta V_{in} Q}{64\pi D} \tag{6}$$

$$\eta = 4\pi\gamma^2(\gamma^2 - 1)e_{31,f} z_p, \tag{7}$$

where V_{in} is the voltage applied to the pMUT; Q is the quality factor; η is the electromechanical transformer ratio coefficient; z_p is the distance from the neutral axis to the middle of the piezoelectric layer; $e_{31,f}$ is the intrinsic effective piezoelectric coefficient; and γ is the ratio of the radius between the top electrode to the cavity. Based on previous research, this study used 2 μm as the predefined thickness of the piezoelectric layer and found the radius using Equations (3)-(5) [24]. Since V_{in}, Q, π, R, and $e_{31,f}$ are constants, the relationship between the thickness of the piezoelectric layer and the maximum displacement at the center can be found using Equations (6)-(7).

C. FABRICATION AND CHARACTERIZATION OF A SINGLE pMUT AND A pMUT ARRAY

The process flow of fabricating pMUT with sol-gel PZT thin film as the piezoelectric layer is shown in Figure 5. First, a commercial SOI (silicon-on-insulator) wafer, with 700 μm of bulk silicon, a device layer thickness of 5 μm, and a buried SiO_2 layer of 1 μm, was polished down to 350 μm from the back. Next, a 20 nm Ti adhesion layer and a

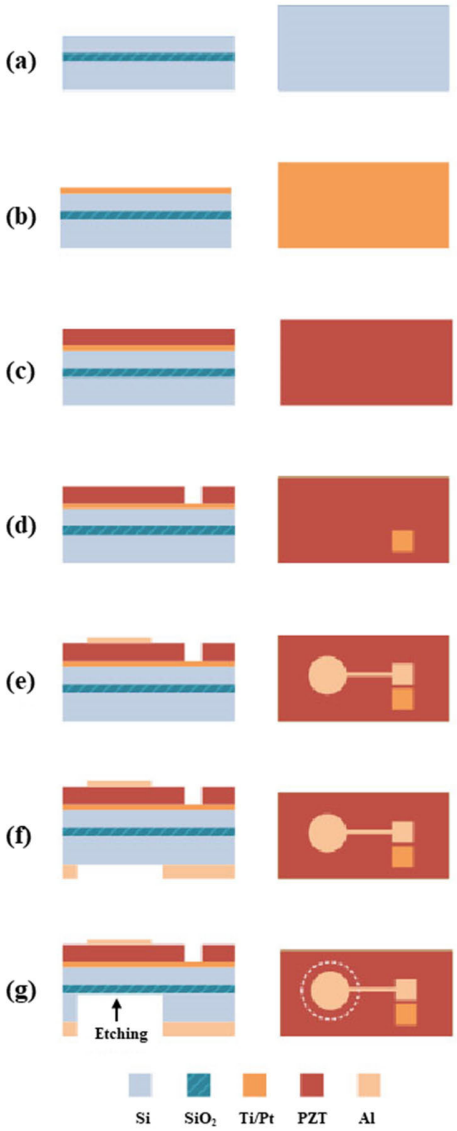

FIGURE 5. **Seven-step process flow for fabricating the proposed pMUT using sol-gel PZT as the actuation layer.**

250 nm Pt bottom electrode layer were deposited by e-beam evaporation. Then, the PZT film was fabricated by sol-gel deposition as mentioned in Section II-A, followed by a two-step wet-etch process to expose the bottom electrode. Next, a 100 nm Al top electrode layer was formed by RF sputtering and patterned using a lift-off process. To etch the cavities on the back, a 500 nm Al mask layer was patterned on the bottom of the wafer using sputtering and lift-off. Afterward, inductively coupled plasma etching (ICP) was used to release the diaphragm from the back side. The deep etching was stopped at the silicon dioxide layer of the SOI. To investigate the feasibility of making a pMUT array with the proposed method, this study established a simulation platform based on k-Wave to evaluate the acoustic pressure of the array.

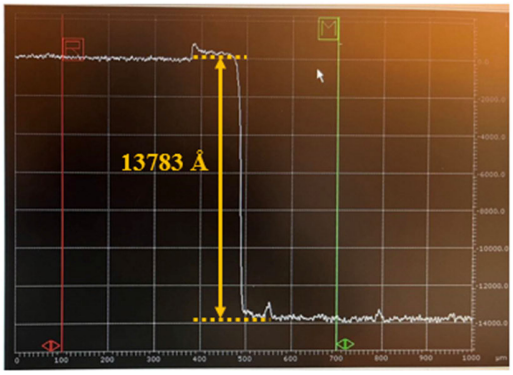

FIGURE 6. **Step height of the 27 layers of PZT thin film.**

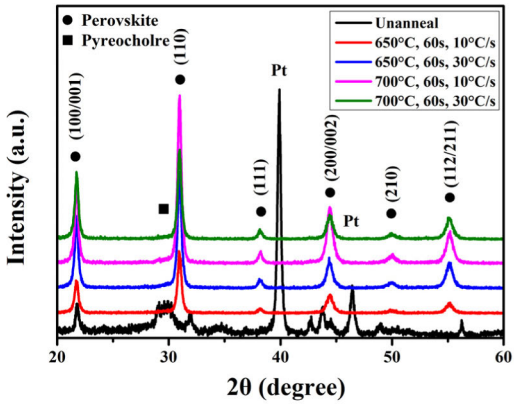

FIGURE 7. **XRD results of PZT thin films subjected to different RTA conditions.**

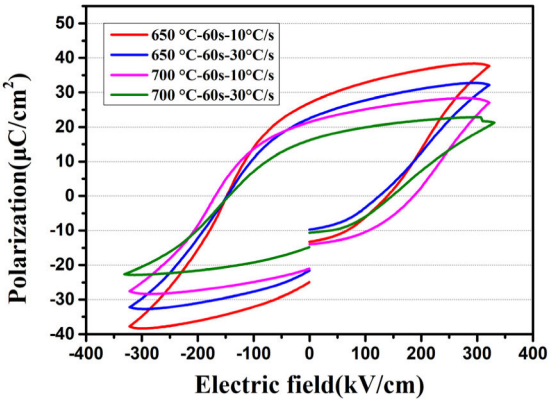

FIGURE 8. **P-E hysteresis loops of the PZT thin films under different annealing conditions (temperature, total time, temperature gradient).**

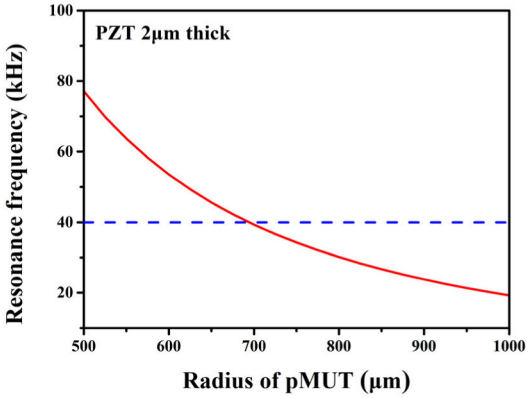

FIGURE 9. **Calculated resonance frequency versus the radius of pMUT actuated by a 2 μm sol-gel PZT thin film.**

In this work, the dimension of the cavity of the pMUT was observed with a 3D laser microscope and a scanning electron microscope (SEM). Besides, the thickness of each layer was observed with SEM at the cross-section cut by a focused ion beam (FIB). Moreover, the resonance frequencies of the pMUTs with different radii under various voltages were measured by the impedance analyzer and the laser Doppler vibrometer (LDV). Furthermore, the acoustic pressure of the pMUT was measured by placing a standard microphone (B&K 4954A) above it.

III. RESULT AND DISCUSSION

A. CHARACTERIZATION of SOL-GEL PZT THIN FILM

As Figure 6 presents, the height of the 27 PZT layers was 13783 Å, with an average thickness of 51.05 nm, which was close to the manufacturer's specification of 47 nm per layer. Figure 7 illustrates the XRD analysis of the PZT samples with different combinations of annealing temperatures and gradients. For the unannealed sample, a pyrochlore peak was found at 2θ of 29°. For the annealed PZT thin films, distinct perovskite phases were observed at 2θ of 22° and 32°, accompanied by a significant reduction of the pyrochlore phase. Hence, after annealing, the pyrochlore phase of all the PZT thin films was transformed into the perovskite phase. Figure 8 presents the remnant polarization results of the sol-gel PZT thin films. The figure clearly shows that the hysteresis loops for the PZT thin film annealed at 650 °C with a temperature gradient of 10 °C/s exhibited significantly higher remnant polarization value (27 μC/cm^2) than those annealed at other temperatures. Therefore, these annealing parameters were selected for fabricating the cantilevers and pMUTs mentioned in Section II-A and II-C, respectively.

To identify the transverse piezoelectric coefficient d_{31}, a 2 μm sol-gel PZT thin film annealed at 650 °C with a temperature gradient of 10 °C/s was deposited on a 20 mm × 3 mm cantilever as shown in Figure 2. The maximum displacement of the cantilever's tip was 418 nm, measured by the LDV when driving with a 100 V_{pp} sinusoidal signal. The frequency of the driving signal was 100 Hz, significantly lower than the cantilever's resonance frequency. The s_{11}^E of the silicon was set to 13.8 pm^2/N and s_{12}^E to 17.1 pm^2/N based on previous research [25]. Per Equation (1), the transverse piezoelectric coefficient d_{31} of the fabricated PZT thin film was -33.9 pC/N which was close to what previous studies had reported (-5 to -59.9 pC/N) [25], [26], [27].

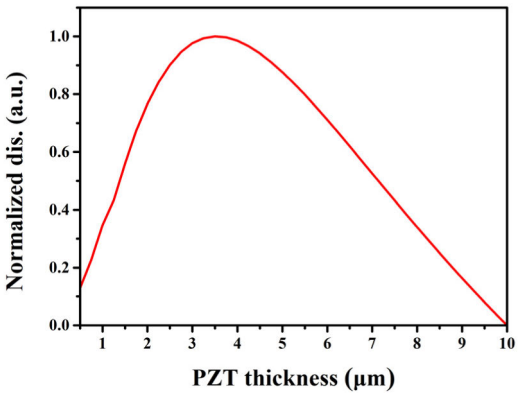

FIGURE 10. **Normalized displacement versus PZT thickness varying from 1 μm to 10 μm.**

TABLE 1. **Material properties of each layer for pMUT modeling.**

	SiO_2	Si	PZT	Al	Pt
Young's modulus E (GPa)	70	170	61.5	70	168
Poisson's ratio v	0.17	0.28	0.394	0.35	0.38
Density ρ (kg/m^3)	2200	2329	7500	2700	21450

B. MODELING OF THE pMUT

Figure 9 displays the simulated resonance frequencies corresponding to different radii of pMUTs that used the 2 μm sol-gel PZT thin film. The material properties for each layer are shown in Table 1. Considering the Ti layer was only 20 nm, the bottom electrode layer was reduced to 250 nm of Pt. The simulation results indicated that a pMUT with a radius of 694 μm would have a resonant frequency of 40 kHz. Therefore, this study fabricated the pMUTs with radii ranging from 550 μm to 775 μm. In addition, the relationship between the maximum displacement in the center of the pMUT and the PZT thickness was calculated using Equations (6)-(7), as shown in Figure 10. It was observed that the maximum displacement in the center of the pMUT increased with the PZT thickness until the latter exceeded 3.5 μm. Hence, this study also fabricated a pMUT with a 1μm PZT layer to verify the simulation results.

C. CHARACTERIZATION OF SOL-GEL PZT-BASED AIR-COUPLED pMUT

Figure 11 shows the front and back of the pMUT chip, which demonstrates good fabrication. Since the size of the cavity, etching depth, and thickness of each layer all affect the resonant frequency of the pMUT, this study inspected the dimension of the cavity and etching profile using the 3D laser microscope and SEM, respectively. Figure 12 displays the results from the 3D laser microscope, revealing that the measured radii were close to the designs. Figure 13 shows the SEM image from the back side of the pMUT. The smoothness of the surface indicated that the SiO_2 stopped

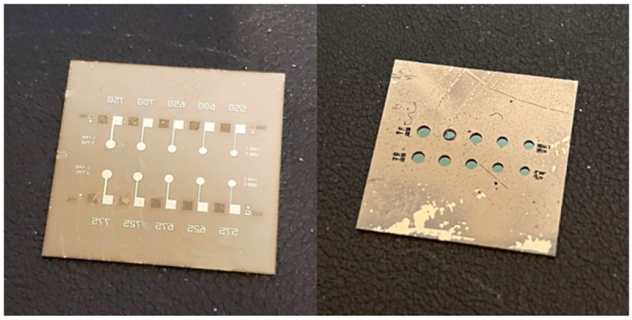

FIGURE 11. **Photo of (a) the front of the pMUTs and (b) the cavities on the back.**

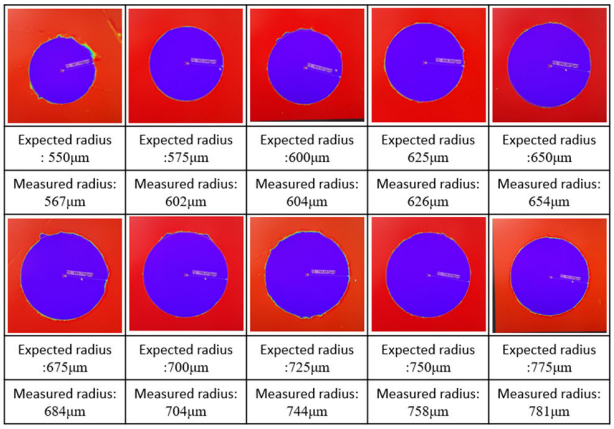

FIGURE 12. **Three-dimensional laser image of the back of the pMUTs whose radii ranged from 550 μm to 775 μm after the etching process of the silicon.**

the ICP etching successfully. Figure 14 displays the SEM image of the cross-sections of the pMUT (cut by FIB). The thickness of each layer was close to the intended deposited thickness, except for the bottom electrode. The expansion of the bottom electrode was due to the leakage of the oxygen molecular when the PZT thin film was annealed. The leaked oxygen molecule oxidized the titanium and caused an increase in thickness. Figure 15 illustrates the measured resonance frequencies of 48 pMUTs with radii varying from 550 μm to 775μm using the impedance analyzer. The results showed that the measured and simulated resonance frequencies were similar. Besides, the proposed pMUT with a radius of 625um had an effective electromechanical coupling factor (keff) of 0.18, which was better than that of previous similar research [19]. Figure 16 presents the measured results using the frequency sweep mode of LDV, which indicates the bandwidth of a 725 μm radius pMUT was 1.9 kHz with a resonance frequency of 34.94 kHz.

As mentioned in Section II-C, we also prepared some pMUTs with a sol-gel PZT layer that was 1 μm thick to compare the acoustic output pressure. As Figure 17 presents the acoustic pressures measured by a microphone at 3 cm

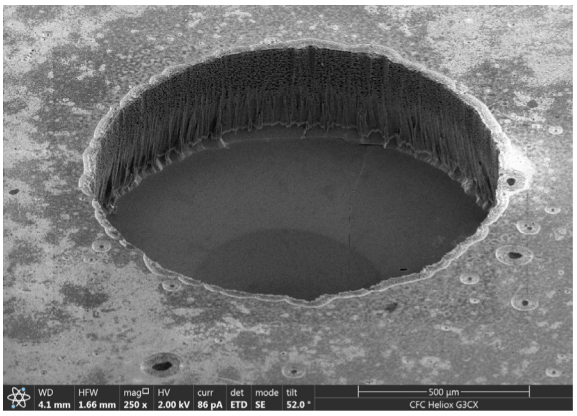

FIGURE 13. **Microstructure SEM images of a cavity on the back of the 550 μm pMUT.**

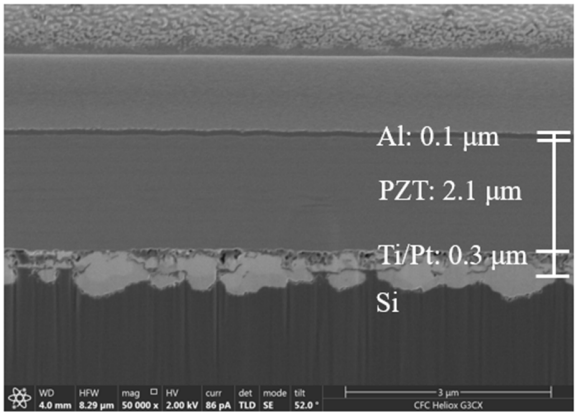

FIGURE 14. **Cross-sectional image of a pMUT with a PZT layer estimated to be 2 μm.**

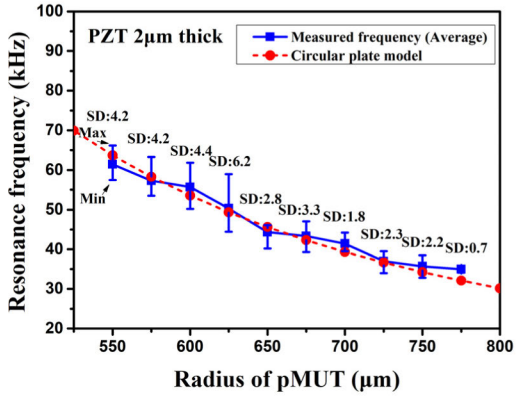

FIGURE 15. **Comparison of measured resonant frequency and simulation result of the 2 μm PZT pMUTs with various radii and a 10 V_{pp} driving voltage.**

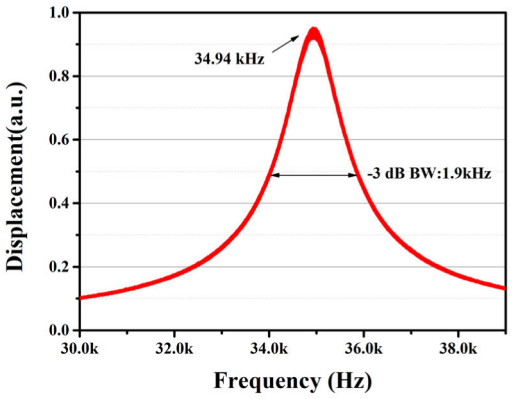

FIGURE 16. **LDV measurement of a 725 μm radius pMUT with a 10 V_{pp} driving voltage. The resonance frequency is 34.94 kHz, and the device bandwidth is 1.9 kHz.**

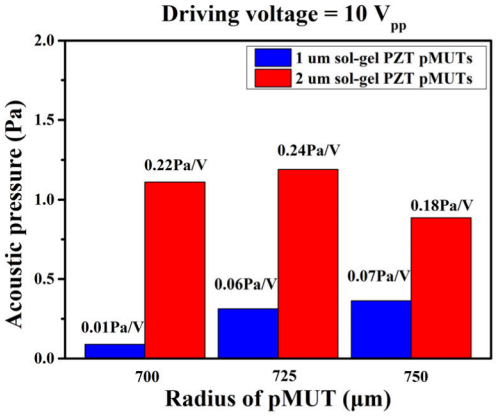

FIGURE 17. **Amplitudes and efficiencies of the output acoustic pressures for the pMUTs with 1 μm versus 2 μm PZT thin film when driven with 10 V_{pp}, 150 sinusoidal burst cycles at their resonance frequencies.**

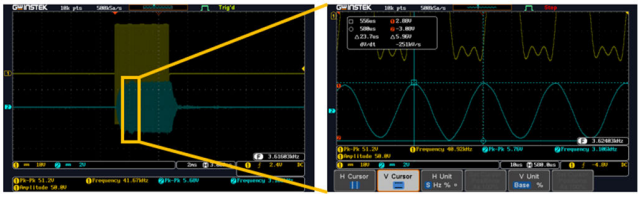

FIGURE 18. **The 725 μm pMUT was driven by the 50 V_{pp} burst signal with 150 cycles sine waves.**

above the pMUTs with radii of 700 μm, 725 μm, and 750 μm. During the measurement, the pMUTs were driven by a 10 V_{pp}, 150 cycles sinusoidal burst signal at their resonance frequencies. The pMUTs with 2 μm PZT exhibited a sound pressure at least 2.4 times greater than those with 1 μm PZT, consistent with the simulated results shown in Figure 10. Additionally, the driving voltage was increased to 50 V_{pp}, and the maximum acoustic pressure was 4.42 Pa from the pMUT with a radius of 725 μm, as shown in Figure 18. The driving and received signals were on the top and bottom of the screen, respectively. Figure 19 shows that as the driving voltage increased, the output efficiency of the pMUT (whether the radius was 700 μm or 725 μm) decreased and the resonant frequency increased. As Figure 20 displays, the peak-to-peak displacement in the center of the pMUT was

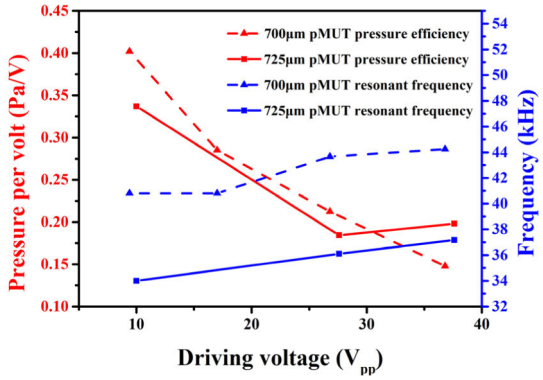

FIGURE 19. **Pressure output efficiency and resonant frequencies of the 700 μm and 725 μm pMUTs corresponding to the different driving voltages (V_{pp}), measured with a standard microphone and LDV, respectively.**

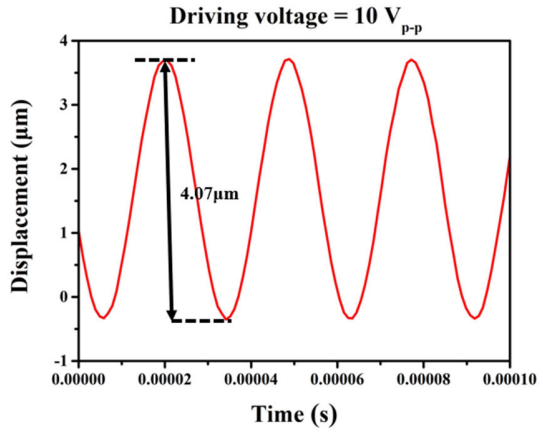

FIGURE 20. **Displacement signal of the 725 μm pMUT measured with an LDV.**

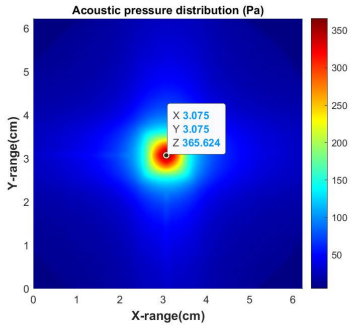

FIGURE 21. **Simulated acoustic pressure distribution of the focal plane (3 cm above the array) of an 11 × 11 pMUT array. The radius of the pMUT was 725 μm, and the element pitch was 1700 μm.**

4.07 μm when the input signal was 10 V_{pp} at its resonance frequency, which was close to the thickness of the stack. Hence, this phenomenon could be attributed to the nonlinear spring hardening effect when the membrane deflection is close to its thickness [13], [28].Finally, the pMUT's maximum output acoustic pressure (4.42 Pa) was used to evaluate the output of a pMUT array with sol-gel PZT as the actuation layer. As mentioned in Section II-C, the pMUT array was simulated using the k-Wave toolbox. An 11×11 array of 725 μm pMUTs was placed in an 18.45 mm × 18.45 mm region. The focal point was set to 3 cm above the array's center. The simulated distribution of sound pressure at the height of the focal point is shown in Figure 21. The pressure at the focal point was 365.624 Pa, which exceeded the minimum required pressure (338 Pa) for ultrasonic haptic feedback [7]. Since ultrasound haptic feedback is commonly considered the most demanding mid-air ultrasound application in terms of the required acoustic pressure, this study confirmed the feasibility of using the sol-gel method to prepare PZT-based pMUTs for more mid-air applications.

IV. CONCLUSION

The existing air-coupled ultrasonic transducers are bulky and require expensive equipment to deposit PZT thin films. This research provides a solution by demonstrating a novel method of producing air-coupled pMUTs that uses sol-gel PZT with good reliability and low facility demand. First, the deposition process of the PZT thin film using the sol-gel method was optimized. The d_{31} of the proposed PZT thin film was −33.9 pC/N. Next, the dimension of the pMUTs was determined using a circular plate model. Eventually, the fabricated pMUTs were measured and found to be consistent with the simulation. Among them, the pMUT with a radius of 725 μm had a maximum output pressure of 4.42 Pa at 3 cm above it when driven by a 50 Vpp sinusoidal wave at 40.48 kHz. To further investigate the output pressure of the pMUT array, a k-Wave model was built with 11 × 11 725 μm pMUTs inside an 18.45 mm × 18.45 mm area. When focusing the acoustic waves at 3 cm above the virtual pMUT array, the simulated output acoustic pressure reached 365.624 Pa. This result meets the criteria of generating tactile sensation using ultrasonic waves. Hence, the proposed method could also apply to other mid-air ultrasonic applications with lower requirements on acoustic pressures, such as object detection and particle manipulation. In conclusion, this work demonstrated the first air-coupled pMUTs using sol-gel PZT and revealed its potential for mid-air ultrasound applications.

REFERENCES

[1] B. W. Drinkwater and P. D. Wilcox, "Ultrasonic arrays for non-destructive evaluation: A review," *NDT E Int.*, vol. 39, no. 7, pp. 525–541, Oct. 2006, doi: 10.1016/j.ndteint.2006.03.006.

[2] X. Jiang, K. Kim, S. Zhang, J. Johnson, and G. Salazar, "High-temperature piezoelectric sensing," *Sensors*, vol. 14, no. 1, pp. 144–169, Dec. 2013. [Online]. Available: https://www.mdpi.com/1424-8220/14/1/144

[3] I. Donald, J. Macvicar, and T. G. Brown, "Investigation of abdominal masses by pulsed ultrasound," *Lancet*, vol. 271, no. 7032, pp. 1188–1195, Jun. 1958, doi: 10.1016/S0140-6736(58)91905-6.

[4] A. Fenster and D. B. Downey, "3-D ultrasound imaging: A review," *IEEE Eng. Med. Biol. Mag.*, vol. 15, no. 6, pp. 41–51, Nov. 1996, doi: 10.1109/51.544511.

[5] Y. Qiu et al., "Piezoelectric micromachined ultrasound transducer (PMUT) arrays for integrated sensing, actuation and imaging," *Sensors*, vol. 15, no. 4, pp. 8020–8041, Apr. 2015. [Online]. Available: https://www.mdpi.com/1424-8220/15/4/8020

[6] G. R. T. Haar, "High intensity focused ultrasound for the treatment of tumors," *Echocardiography*, vol. 18, no. 4, pp. 317–322, May 2001, doi: 10.1046/j.1540-8175.2001.00317.x.

[7] T. Howard, G. Gallagher, A. Lécuyer, C. Pacchierotti, and M. Marchal, "Investigating the recognition of local shapes using mid-air ultrasound haptics," in *Proc. IEEE World Haptics Conf. (WHC)*, Jul. 2019, pp. 503–508, doi: 10.1109/WHC.2019.8816127.

[8] A. Halbach et al., "Display compatible PMUT array for mid-air haptic feedback," in *Proc. 20th Int. Conf. Solid-State Sensors, Actuat. Microsyst. Eurosensors (TRANSDUCERS EUROSENSORS XXXIII)*, Jun. 2019, pp. 158–161, doi: 10.1109/TRANSDUCERS.2019.8808775.

[9] A. Marzo, T. Corkett, and B. W. Drinkwater, "Ultraino: An open phased-array system for narrowband airborne ultrasound transmission," *IEEE Trans. Ultrason., Ferroelectr., Freq. Control*, vol. 65, no. 1, pp. 102–111, Jan. 2018.

[10] R. J. Przybyla, H.-Y. Tang, A. Guedes, S. E. Shelton, D. A. Horsley, and B. E. Boser, "3D ultrasonic rangefinder on a chip," *IEEE J. Solid-State Circuits*, vol. 50, no. 1, pp. 320–334, Jan. 2015, doi: 10.1109/JSSC.2014.2364975.

[11] T. Wang, T. Kobayashi, and C. Lee, "Highly sensitive piezoelectric micromachined ultrasonic transducer operated in air," *Micro Nano Lett.*, vol. 11, no. 10, pp. 558–562, Oct. 2016, doi: 10.1049/mnl.2016.0207.

[12] T. Wang, T. Kobayashi, B. Yang, H. Wang, and C. Lee, "Highly sensitive piezoelectric micromachined ultrasonic transducer (pMUT) operated in air," in *Proc. IEEE 11th Annu. Int. Conf. Nano/Micro Eng. Mol. Syst. (NEMS)*, Apr. 2016, pp. 294–299, doi: 10.1109/NEMS.2016.7758253.

[13] G.-L. Luo, Y. Kusano, and D. A. Horsley, "Airborne piezoelectric micromachined ultrasonic transducers for long-range detection," *J. Microelectromech. Syst.*, vol. 30, no. 1, pp. 81–89, Feb. 2021, doi: 10.1109/JMEMS.2020.3037298.

[14] C. H. Huang et al., "Design, modelling, and characterization of display compatible pMUT device," in *Proc. 19th Int. Conf. Thermal, Mech. Multi-Phys. Simulation Exp. Microelectron. Microsyst. (EuroSimE)*, Apr. 2018, pp. 1–4, doi: 10.1109/EuroSimE.2018.8369931.

[15] T. J. Zhu, L. Lu, and M. O. Lai, "Pulsed laser deposition of lead-zirconate-titanate thin films and multilayered heterostructures," *Appl. Phys. A, Solids Surf.*, vol. 81, no. 4, pp. 701–714, Sep. 2005, doi: 10.1007/s00339-005-3227-z.

[16] D. Ambika, V. Kumar, H. Imai, and I. Kanno, "Sol-gel deposition and piezoelectric properties of {110}-oriented $Pb(Zr_{0.52}Ti_{0.48})O_3$ thin films," *Appl. Phys. Lett.*, vol. 96, no. 3, Jan. 2010, Art. no. 031909, doi: 10.1063/1.3293446.

[17] G. Tan, S.-H. Kweon, and I. Kanno, "Piezoelectric properties of epitaxial $Pb(Zr,Ti)O_3$ thin films grown on Si substrates by the sol–gel method," *Thin Solid Films*, vol. 764, Jan. 2023, Art. no. 139612, doi: 10.1016/j.tsf.2022.139612.

[18] B. Belgacem, F. Calame, and P. Muralt, "5I-2 thick PZT sol-gel films for pMUT transducers performances improvement," in *Proc. IEEE Ultrason. Symp.*, Apr. 2006, pp. 926–929, doi: 10.1109/ULTSYM.2006.247.

[19] Y.-Q. Chen et al., "Large-scale and high-density pMUT array based on isolated sol-gel PZT membranes for fingerprint imaging," *J. Electrochem. Soc.*, vol. 164, no. 7, pp. B377–B381, 2017.

[20] C. Yan, Y. Minglei, Z. Qunying, C. Xiaolong, C. Jinkui, and G. Le, "Properties of RF-sputtered PZT thin films with Ti/Pt electrodes," *Int. J. Polym. Sci.*, vol. 2014, pp. 1–5, Jan. 2014, doi: 10.1155/2014/574684.

[21] L.-P. Wang, R. Wolf, Q. Zhou, S. Trolier-McKinstry, and R. J. Davis, "Wet-etch patterning of lead zirconate titanate (PZT) thick films for microelectromechanical systems (MEMS) applications," *MRS Proc.*, vol. 657, p. EE539, Jan. 2000, doi: 10.1557/proc-657-ee5.39.

[22] D.-M. Chun, M. Sato, and I. Kanno, "Precise measurement of the transverse piezoelectric coefficient for thin films on anisotropic substrate," *J. Appl. Phys.*, vol. 113, no. 4, Jan. 2013, Art. no. 044111, doi: 10.1063/1.4789347.

[23] C. H. J. Fox, X. Chen, and S. McWilliam, "Analysis of the deflection of a circular plate with an annular piezoelectric actuator," *Sens. Actuators A, Phys.*, vol. 133, no. 1, pp. 180–194, Jan. 2007.

[24] D. Horsley, Y. Lu, and O. Rozen, "Flexural piezoelectric resonators," in *Piezoelectric MEMS Resonators*, H. Bhugra and G. Piazza, Eds. Cham, Switzerland: Springer, 2017, pp. 153–173.

[25] P. M. Mayrhofer, E. Wistrela, M. Schneider, A. Bittner, and U. Schmid, "Precise determination of d_{33} and d_{31} from piezoelectric deflection measurements and 2D FEM simulations applied to $Sc_xAl_{1-x}N$," *Proc. Eng.*, vol. 168, pp. 876–879, Dec. 2016, doi: 10.1016/j.proeng.2016.11.295.

[26] J. Tsaur, Z. J. Wang, L. Zhang, M. Ichiki, J. W. Wan, and R. Maeda, "Preparation and application of lead zirconate titanate (PZT) films deposited by hybrid process: Sol-gel method and laser ablation," *Jpn. J. Appl. Phys.*, vol. 41, no. 11B, pp. 6664–6668, Nov. 2002, doi: 10.1143/jjap.41.6664.

[27] A. Schroth, C. Lee, S. Matsumoto, M. Tanaka, and R. Maeda, "Application of sol-gel deposited thin PZT film for actuation of 1D and 2D scanners," in *Proc. IEEE 11th Annu. Int. Workshop Micro Electro Mech. Syst., Invest. Micro Struct., Sensors, Actuat., Mach. Syst.*, Jan. 1998, pp. 402–407, doi: 10.1109/MEMSYS.1998.659790.

[28] I. O. Wygant, M. Kupnik, and B. T. Khuri-Yakub, "An analytical model for capacitive pressure transducers with circular geometry," *J. Microelectromech. Syst.*, vol. 27, no. 3, pp. 448–456, Jun. 2018, doi: 10.1109/JMEMS.2018.2823200.

YA-HAN LIU (Graduate Student Member, IEEE) was born in Yunlin, Taiwan, in 1993. She received the bachelor's and master's degrees from the Department of Electrical Engineering, National Cheng Kung University, Tainan, Taiwan, in 2015 and 2018, respectively, where she is currently pursuing the Ph.D. degree with the Institute of Microelectronics. Her research interests include large-area electronics and MEMS device development for various applications.

HSIAO-CHI LIN was born in Keelung, Taiwan, in 1996. She received the bachelor's degree from the Department of Electrical Engineering, National University of Tainan, Tainan, Taiwan, in 2020, and the master's degree from the Department of Electrical Engineering, National Cheng Kung University, in 2023. Her research interests include piezoelectric micromachined ultrasonic transducer and its application on ultrasound haptic applications.

CHIH-YING LI was born in Taipei, Taiwan, in 1997. She received the bachelor's degree from the Department of Mechanical Engineering, National Cheng Kung University, Tainan, Taiwan, in 2020, and the master's degree from the Department of Electrical Engineering, National Cheng Kung University, in 2023. Her research interests include algorithm development and system setup for photoacoustic imaging reconstruction.

CHIEN-LUN KAO, photograph and biography not available at the time of publication.

HAN-JEN HSU was born in Taipei, Taiwan, in 1998. He received the bachelor's degree from the Department of Mechanical Engineering, National Central University, Taoyuan, Taiwan, in 2021. He is currently pursuing the master's degree in electrical engineering with the National Cheng Kung University. His research interests include the development of MEMs and pMUTs fabrication.

YEONG-HER WANG (Life Member, IEEE) received the B.S. and Ph.D. degrees in electrical engineering from the National Cheng Kung University (NCKU), Tainan, Taiwan, in 1978 and 1985, respectively. He is currently a Distinguished Professor with the Department of Electrical Engineering, Institute of Microelectronics; and the Department of Photonics, NCKU. His research and teaching activities have focused on semiconductor devices and physics, in the development and modeling of III–V compound semiconductor devices. His current interests include developing new techniques for oxide materials for III–V based metal-oxide-semiconductor or heterostructure FETs and also responsible for the MMIC design and fabrication, especially for high power MMIC by AlGaN/GaN HEMT devices.

CHIH-HSIEN HUANG (Member, IEEE) was born in Taichung, Taiwan, in 1981. He received the bachelor's and master's degrees from the Department of Electrical Engineering, National Cheng Kung University, Tainan, Taiwan, and the Ph.D. degree in electrical and computer engineering from Texas A&M University, College Station, TX, USA, in 2015. From 2005 to 2010, he was with the Industrial Technology Research Institute, Tainan, as a Research and Development Engineer. In 2010, he was a Research Assistant with the Department of Electrical and Computer Engineering, Texas A&M University. From 2015 to 2016, he was a Research, Design, and Development Engineer with Baker Hughes Incorporated, Houston, TX. From 2017 to 2018, he held a postdoctoral position with IMEC, Belgium. He is currently an Associate Professor with the Department of Electrical Engineer, NCKU. He has published about 40 papers on international journals and proceedings of peer reviewed conferences along with ten patents (US, CN, and TW). His research interests include design, simulation, and characterization of acoustic MEMS devices, such as pMUT, MEMS acoustic mirror, and photoacoustic transducer. Besides, he also worked on Acoustic Tomography with 2-D ultrasound transducer array for NDT.